COBEM 2021 26th International Congress of Mechanical Engineering
November 22-26, 2021, Virtual Congress, Brazil
ABCM Associação Brasileira de Engenharia e Ciências Mecânicas

COB-2021-0750
Numerical study of the flow past an inclined flat plate via spectral/hp element methods with novel stabilization

Yukari W. G. Martins
Vinicius Malatesta
Rodrigo C. Moura
Instituto Tecnológico de Aeronáutica (ITA), São José dos Campos, São Paulo, 12228-900, Brasil
yukari.martins@ga.ita.br

Abstract. *This study is devoted to the analysis of the flow past an inclined flat plate simulated with the high-order spectral/hp continuous Galerkin (CG) method at a moderate Reynolds number. A novel numerical stabilization strategy is employed, in which the jump (i.e. discontinuous variation) of the solution's derivative across element interfaces is penalized. Since CG's solution is by construction only C^0 continuous at interfaces, the jump in question indicates the degree of numerical under-resolution, serving as a natural sensor for stabilization. Although the base strategy is not new, it is here applied with novel adaptations that make it suitable for the simulation of transitional and turbulent flows. Still, although Reynolds numbers typical of turbulent wakes are considered, focus is given to two-dimensional simulations due to the pioneering character of the study. These cases are nevertheless already unstable without added stabilization, owing to CG's high-order character. Relevant flow characteristics are compared with those obtained in previous works for the sake of validation.*

Keywords: *spectral element method, high-order numerical methods, inclined flat plate, asymmetric vortex shedding*

1. INTRODUCTION

Bluff bodies under turbulent flow have been extensively studied experimentally and numerically because of their wide application in engineering (Lam and Wei, 2010). The vortex shedding behind an inclined plate has complex characteristics and different scales to be resolved, making it a rich case of study. This flow has already been investigated by different methods in the literature (Breuer and Jovicic, 2001; Lam and Wei, 2010; Li *et al.*, 2017), although several aspects can still be further explored. Still, the previous works serve as reference for subsequent studies, such as the present one.

Turbulent flows involve a wide range of spatial and temporal scales, thus requiring a significant amount of computational resources when it comes to high-fidelity simulations (Amor *et al.*, 2020). Computational fluid dynamics (CFD) has evolved over the years due to improved numerical algorithms and computational power. Beyond that, we can also mention the improvement in CFD mesh generators, turbulence models and flow visualization techniques. In particular, the development of high-order methods in CFD (Wang, 2007) has brought a significant gain in terms of simulation efficiency, especially for transitional and turbulent flows. The so-called spectral elements methods (SEM), see e.g. Karniadakis and Sherwin (2013), are an important part of this evolution, as they integrate high accuracy with geometrical flexibility.

Amongst a variety a SEMs, the spectral/hp continuous Galerkin (CG) method (Xu *et al.*, 2018), arguably the most popular SEM when it comes to incompressible flows, has received significant attention over recent years with regards to appropriate numerical stabilisation for under-resolved turbulent flows. In these approaches, meshes typical of large-eddy simulation (LES) are employed, but no turbulence model is added explicitly. Although this approach is often called implicit LES, cf. e.g. Lombard *et al.* (2016), the term under-resolved DNS (as in direct numerical simulation of turbulence) has also been advocated (Moura *et al.*, 2015, 2017) and is preferred in the present work. In any case, this strategy requires a delicate balance between stability (numerical robustness) and accuracy (solution quality).

A technique that has been proven specially useful in achieving the balance mentioned above is the so-called spectral vanishing viscosity (SVV), cf. Kirby and Sherwin (2006), in which a hiperviscosity-type term is added to the governing equations. Although significant improvements have been incorporated into modern SVV operators (Moura *et al.*, 2016), some issues still remain. For example, in the most recent version of the technique developed for under-resolved flows (Moura *et al.*, 2020a), SVV's numerical dissipation was found to be sub-optimal, essentially reducing by one the order of accuracy expected from the method.

This study aims at testing a different stabilization technique that, at least upon linear dispersion/diffusion analysis (Moura *et al.*, 2020b), is supposed to deliver a superior performance than that of SVV as in Moura *et al.* (2016, 2020a). This type of linear analysis has been proven surprisingly useful in providing insights for under-resolved nonlinear simulations, including turbulent flows (Mengaldo *et al.*, 2018b; Fernandez *et al.*, 2019). In any case, the stabilization technique

employed here is that originally developed in Burman (2007); Burman and Fernández (2009); Burman (2015), but here applied with adaptations that make it suitable for transitional/turbulent flows.

This adapted technique is called GJP (gradient-jump penalty) stabilization, as it penalizes the jump (discontinuous variation) of the solution's derivative across element interfaces. Since CG's numerical solution is only C^0 continuous at interfaces, the gradient jump serving as a natural sensor for under-resolution. The adaptation considered here concerns basically the appropriate choice of GJP's penalty parameter, as informed through linear dispersion/diffusion analysis. More specifically, the linear analysis is used to find, for each CG discretization order, the GJP parameter that yields the best dissipation profile. This choice takes into account aspects such as dissipation scaling, overall magnitude and monotonicity, i.e. dissipation should only increase with frequency.

Another important aspect for under-resolved DNS approaches based on SEMs is that of computational efficiency. This has been measured in many recent works in terms of resolution power (or eddy-resolving capability) per DOFs (degrees of freedom) employed, see e.g. Lombard *et al.* (2016); Moura *et al.* (2016, 2020a). GJP's linear dispersion/diffusion analysis (Moura *et al.*, 2020b) points out that, even at large frequencies (small scales), CG's resolution power per DOF should increase with its discretization order (or polynomial order). This suggests that GJP-stabilized CG should yield superior solution quality for multi-scale flows at higher discretization orders. This is also tested in the present work by test cases that combine coarser meshes with higher element-wise polynomial orders (or vice-versa), this way maintaining the total number of DOFs approximately fixed. To that end, we use carefully designed meshes that feature both unstructured and structured patterns.

As mentioned in the beginning, the flow case under study is that of an inclined flat plate with either sharp or rounded edges, considered at Reynolds number $Re = 1000$. Due to the exploratory character of the study, focus is given to two-dimensional simulations. These are conducted through the incompressible CG solver available in the $Nektar$++ platform (Cantwell *et al.*, 2015; Moxey *et al.*, 2020). Aspects of flow physics are also analyzed and compared with those obtained in previous works.

This paper is organized as follows. Section 2 introduces the numerical method employed and the GJP stabilization technique. Section 3 addresses the mesh generation strategy and the test cases considered. Section 4 covers the results of the main simulations and the relevant flow quantities obtained. Lastly, our conclusions are summarized in Section 5.

2. NUMERICAL METHOD AND STABILIZATION

The spectral/hp continuous Galerkin (CG) method works with element-wise solutions in the form

$$u^{\,e}(\boldsymbol{x},t) \;= \sum_{j=0}^{p} \hat{u}_j^{\,e}(t)\,\varphi_j(\boldsymbol{\xi}(\boldsymbol{x}))\;, \tag{1}$$

where e denotes the element under consideration and $\hat{u}_j^{\,e}$ are its time-dependent solution coefficients, which accompany the corresponding basis functions $\varphi_j(\boldsymbol{\xi})$ making up a polynomial element-wise solution of order p. These lead to CG discretizations with nominal order of accuracy of $p+1$. The modified Legendre basis functions defined in Karniadakis and Sherwin (2013) have been adopted in the present work. Basis functions can be defined in the standard reference space $\boldsymbol{\xi}$ and then employed to describe element-wise solutions in the physical space $\boldsymbol{x}$ via mapping relations, as also described in Karniadakis and Sherwin (2013). The subsequent solution strategy is not fundamentally different than that of traditional finite element methods, except that special basis functions are used in order to achieve discretizations of higher order in an efficient manner. In addition, high-order CG usually requires a suitable stabilization strategy as discussed below.

In this work, we employ the GJP (gradient-jump penalty) stabilization technique first proposed and developed in Burman (2007); Burman and Fernández (2009); Burman (2015). This strategy consists in adding a (mostly) dissipative term into CG's discretization that penalizes under-resolved parts of the solution. This term is made proportional to the jump (discontinuous variation) of the solution's derivative across element interfaces. Since CG is, by construction, only C^0 continuous at interfaces, this gradient-jump is a natural proxy for under-resolution. The resulting technique thus regularizes under-resolved flow regions by adding a controlled amount of numerical dissipation.

The novelty of the present application of the GJP technique consists in having its dissipation carefully adjusted to the simulation of transitional and turbulent flows. More specifically, we rely on linear dispersion/diffusion analysis to decide which value of GJP's penalty parameter τ yields a suitable dissipation profile for each discretization order. We note that τ is simply the coefficient multiplying the added GJP term. This type of analysis has been used with surprising success in previous works (Moura *et al.*, 2015, 2016; Mengaldo *et al.*, 2018b; Moura *et al.*, 2020b) dealing with under-resolved simulations of turbulence via spectral element methods (SEMs).

The relevant framework for the present work is that of spatial dispersion/diffusion analysis, where inflow/outflow-type boundary conditions are assumed (instead of periodic conditions). In this analysis, one prescribes a real-valued angular frequency ω for a propagating wave-like solution such as

$$u(x,t) = \exp\left[i(\kappa x - \omega t)\right]\,, \tag{2}$$

and seeks to find all possible wavenumbers $\kappa = \kappa(\omega)$ that are consistent with the particular discretization considered. Not rarely, one finds multiple complex-valued wavenumbers for each ω, although only one of them is physical. The other ones are associated to spurious waves that are often strongly damped as they propagate in space. Typically, these are either reflected or transmitted spurious waves that appear in regions where mesh spacing changes rapidly (Mengaldo *et al.*, 2018b; Moura *et al.*, 2020a). Here, focus is given to the numerical characteristics of the physical waves. In any case, the imaginary part of $\kappa(\omega)$ is particularly important because it specifies how waves are dissipated or damped as they propagate in space.

The results now shown have been adapted from a recent research report (Moura *et al.*, 2020b) which describes in detail how the dispersion/diffusion analysis approach can be applied to high-order CG with GJP-based stabilization. All the plots that follow consider the linear advection equation (no physical diffusion present). First, we show an example of sub-optimal dissipation characteristics obtained with a naive (uninformed) choice of τ for CG's $p = 4$ discretization, cf. Fig. 1. This figure shows the imaginary part of κ multiplied by the normalizing factor $\hbar = h/p$ (h being the mesh spacing, assumed constant) *versus* the normalized angular frequency $\varpi = \omega/a$ (a being the advection velocity) again multiplied by $\hbar$, such that both $\kappa\hbar$ and $\varpi\hbar$ are non-dimensional.

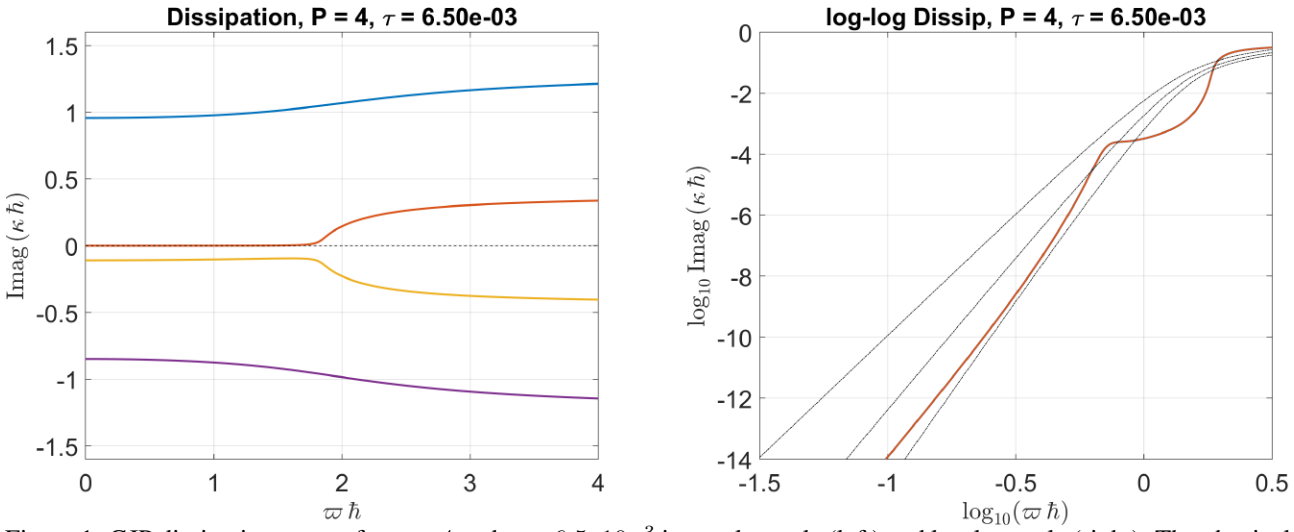

Figure 1: GJP dissipation curves for $p = 4$ and $\tau = 6.5 \cdot 10^{-3}$ in regular scale (left) and log-log scale (right). The physical wave dissipation is shown in red, whereas spurious waves are shown in other colors. For reference, DG dissipation curves are included in the log-log plot at orders $p - 1$, p and $p + 1$ (top to bottom) as black curves.

The left-side plot in Fig. 1 shows the dissipation of the physical wave (red curve) and those of spurious waves (remaining colors), either reflected or transmitted. It should be noted that the physical dissipation is negligible at low-to-moderate frequencies, as it should be (since pure advection is being considered). However, at higher frequencies, it becomes non-negligible (as required for numerical stability). The most important point to be noted is that one of the spurious waves has dissipation close to zero, which means this wave is allowed to survive for some non-negligible time/distance in a simulation. This is not only undesirable for solution quality, but may also lead to instabilities in nonlinear problems (Mengaldo *et al.*, 2018b). Another drawback of this naive choice of τ is that the physical dissipation curve is not as smooth as one could perhaps desire, as more clearly shown in the log-log scale plot. This might lead to undesirable oscillations in the energy spectrum of turbulent flows (Moura *et al.*, 2020a).

We note that the log-log plot includes, for reference, the dissipation curves obtained via standard upwinding in the discontinuous Galerkin (DG) method (Mengaldo *et al.*, 2018a). These are shown as dotted black curves denoting DG's upwind dissipation at orders $p - 1$, p and $p + 1$ (top to bottom, since overall dissipation levels decrease at higher orders).

Finally, we show in Fig. 2 examples of optimal values of τ for CG at $p = 2$, 3 and 5 (top to bottom plots). Moreover, the left-most plots have now been included, and represent the dispersion properties of the stabilized discretization, with the dotted black line indicating the exact dispersion behavior (pure advection). These are the values of τ used in the flow simulations of the present paper, discussed in the next Section.

First, we note that all the dissipation curves of spurious waves have significant dissipation (as they are always far away from the horizontal line marking zero). Secondly, all the physical dissipation curves are significantly smooth (even on the log-log plots). Thirdly, GJP's overall dissipation levels are found to be almost always between those of DG at orders p and $p + 1$, which means that optimal GJP operators seem capable of stabilizing CG while maintaining its accuracy superior to that of same-order (standard upwind) DG.

Lastly, by comparing the physical curves across different polynomial orders, we note that high accuracy (in terms of low dispersion and diffusion errors) is maintained for a larger range of frequencies as p increases. It is important to high-

light that, when comparing plots of different polynomial orders, different mesh sizes must be kept in mind accordingly, so that $\hbar = h/p$ remains fixed. In other words, the usual normalization of dispersion/diffusion plots naturally allows one to compare different discretization orders with the same DOFs. This means, with regards to dissipation curves, that GJP allows for a consistent increase in resolution power (or eddy-resolving capability) per DOF employed as p increases. This property is important in the context of SEM and is not easily achieved with alternative stabilization techniques (Moura *et al.*, 2016, 2020a).

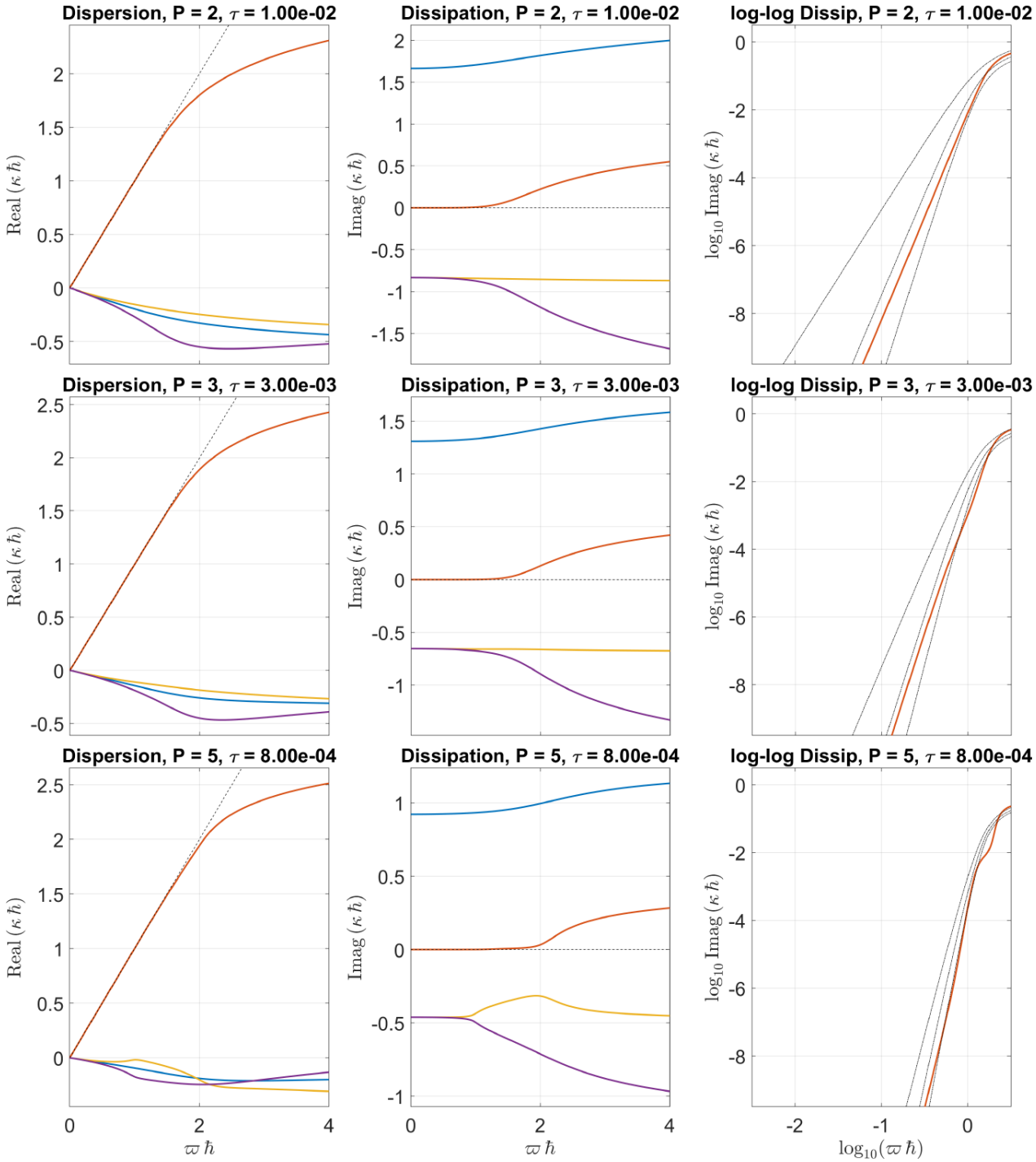

Figure 2: GJP dispersion (left) and dissipation (middle and right) curves for CG at $p = 2$, 3 and 5 (top to bottom). Curves associated to physical waves are shown in red. The remainder of the layout follows that of Fig. 1.

3. MESH GENERATION AND TEST CASES

All simulations relied on 2D meshes generated in Gmsh (Geuzaine and Remacle, 2009), a flexible open source software. The plate has length $L = 1$ and thickness of 2% of L. These dimensions follow the test case studied in Yang *et al.*

(2012), which adopted sharp edges for the plate, so that it is effectively a thin rectangle. The present work focuses mainly on sharp edges, although rounded (semi-circular) edges are also considered in Section 4. In addition, the inclination angle (or angle of attack) for the plate was set to 30^o, also following Yang *et al.* (2012).

All meshes used here have been generated according to the following structure. The inlet region is semi-circular with radius $15L$, see Fig. 3 (left). The center of this semi-circle is also the center of the plate, which is placed already inclined in the domain, so that the freestream enters the domain horizontally. The closure of the domain is made complete by two parallel segments at the top and bottom regions, and by a vertical segment which makes the outflow boundary. These are placed in such a way that makes the domain essentially fit into a square of side $30L$. The plate is enclosed within a circle of radius $2L$, see Fig. 3 (right), while the circle itself is enclosed within a structured region whose shape matches that of the domain's closure. In fact, this structured region has an inverted "D" shape and fits inside a square of side $10L$, whose right-most boundary is shared with the wake region and defines its vertical size. This size was chosen in order to guarantee that wake vortices stay within the wake region which is structured. The wake region has also a square-shaped closure (side $10L$) and its rightmost border touches the outflow boundary of the domain. Its elements are equispaced in the vertical direction and stretch according to a geometric progression along the horizontal direction.

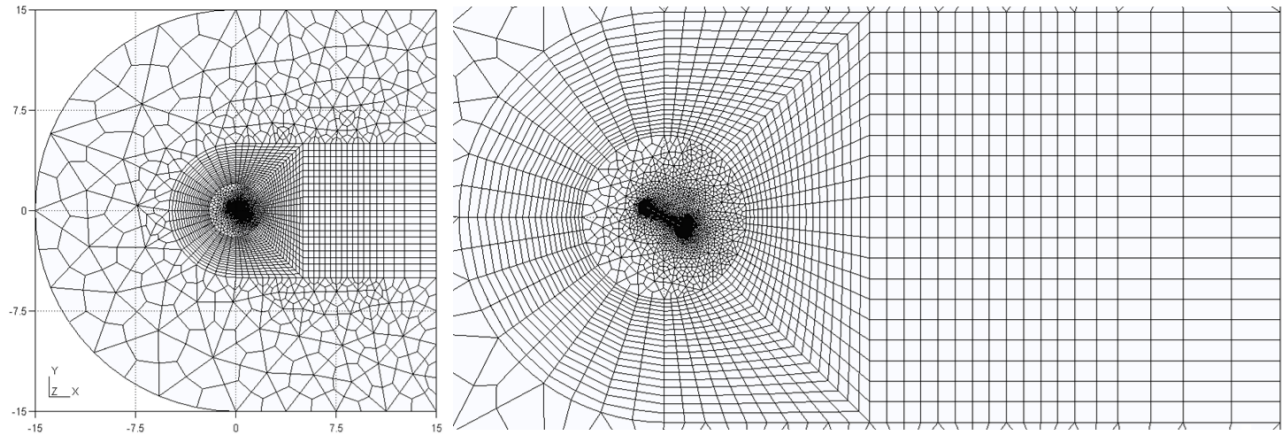

Figure 3: Global view of the mesh (left) and zoomed view showing plate and wake regions (right).

As clearly shown in Fig. 3, the mesh combines regions of structured and unstructured patterns. Still, only quadrilateral elements are employed, since the current version of the GJP stabilization technique is only available for quadrilaterals, although its extension to triangles is well underway. In the unstructured regions, quadrilaterals are made from an initial triangulation of the region followed by a splitting of each triangle into three quadrilaterals. This procedure guaranteed that no triangular elements remained in the mesh, while also allowing for a decent quality of the quadrilateral elements in the unstructured regions. A structured region was also generated to capture the (laminar) boundary layer around the plate, as seen in Fig. 4, which shows this region for both the sharp- and round-edged plate cases. We highlight that both plates have exactly length L, including the edges. The dimensions of the structured boundary layer region have been estimated with formulas for laminar boundary layer thicknesses and have been found adequate for the actual boundary layer profiles observed *a posteriori* in the simulations.

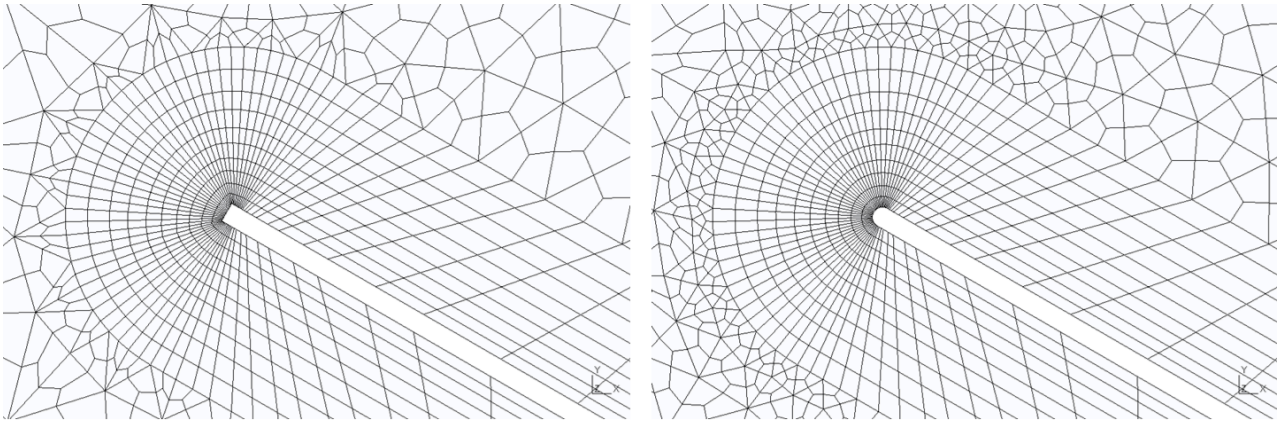
Figure 4: Zoomed view of the plate's leading edge for the sharp (left) and rounded (right) cases.

A mesh refinement study was conducted with three meshes whose parameters are given in Table 1, where N denotes the total number of mesh elements, N_b represents the number of elements (layers) employed across the boundary layer

thickness, whereas N_y and N_x denote the number of elements composing the wake region along respectively the vertical and horizontal directions. For this mesh refinement study, the polynomial order was set to $P = 3$. Different polynomial orders, however, will be considered further below in a subsequent (complementary) analysis.

Table 1: Parameters of the grids used in the mesh refinement study

Grids	N	Domain's side	N_b	N_y	N_x
Cheap grid	4301	$30L$	20	10	30
Medium grid	7722	$30L$	40	20	40
Expensive grid	12044	$60L$	40	20	50

The quantities assessed in the mesh refinement study were (the mean and RMS fluctuation values of) the drag and lift coefficients, defined as $C_D = F_D/(0.5\rho U_0^2 L)$ and $C_L = F_L/(0.5\rho U_0^2 L)$, where F_D and F_L denote respectively the drag and lift forces per unit span, while ρU_0^2 is the freestream dynamic pressure. All cases were found to reach a periodic limit cycle after an initial transient, consistent with the results of Yang *et al.* (2012). Hence, the mean values $\overline{C_L}$ and $\overline{C_D}$, as well as the RMS fluctuation values C'_L and C'_D could be evaluated adequately over a single period of the cycle. These are given in Table 2 for each of the three grids.

Table 2: Lift and drag coefficients (mean and RMS fluctuation) values from the mesh refinement study

Grids	$\overline{C_L}$	$\overline{C_D}$	C'_L	C'_D
Cheap grid	2.0600	1.2844	0.4058	0.1422
Medium grid	2.0440	1.2763	0.4093	0.1442
Expensive grid	2.0497	1.2791	0.4069	0.1427

As the largest variation between the values in Table 2 is of less than 1%, one could be satisfied even with the cheapest grid. However, when the vortices in the wake are considered (not shown), the cheapest grid was found to be clearly more diffusive than the other two grids. Still, by comparing the wake vorticity of the two finer grids, the difference was found to be very small, so that the medium grid was adopted for the actual flow simulations (discussed in Section 4).

In addition, a complementary analysis was conducted to assess the most efficient combination between mesh refinement level and element-wise polynomial order. Taking the medium grid selected above as a baseline, two new grids have been considered: one coarser and another finer. These two were then combined respectively with a higher and a lower polynomial order, namely $P = 5$ and $P = 2$ (contrasting with $P = 3$ used with the medium grid), so that the number of total DOFs in the structured regions of all three grids is similar. For example, in the wake region, these three grids have 30, 20 and 12 elements along the y direction, having the corresponding polynomial orders of $P = 2$, 3 and 5, respectively. In other words, all the three grids have 60 DOFs along the vertical direction (in the wake region). This type of comparison is common in the assessment of spectral/hp element methods, cf. e.g. Moura *et al.* (2020a).

The comparison between the three same-DOF test cases mentioned above showed only minor differences in terms of relevant flow quantities. However, for some reason still yet unclear, case $P = 2$ took considerably longer to run, perhaps due to parallel computing inefficiency. Also, this case yielded the worst solution quality of the three (though the difference amongst them was admittedly small). Cases $P = 3$ and $P = 5$ showed similar computational cost per time step, but case $P = 5$ required a somewhat smaller time step value to ensure stability. Hence, polynomial order $P = 3$ was chosen as the most efficient for the desired number of DOFs and adopted for the actual simulations in the remainder of the study.

4. SIMULATION RESULTS

The simulations were performed with the incompressible CG Solver available in the $Nektar$++ platform (Cantwell *et al.*, 2015; Moxey *et al.*, 2020). The flow past an inclined flat plate of 2% thickness with either sharp or round edges was computed at Reynolds number $Re = 1000$ and inclination 30^o with polynomial order $P = 3$ (cubic element-wise solution) and the medium grid introduced in Section 3. The results are compared with those of Yang *et al.* (2012), which however considered only sharp-edged plates.

Regarding boundary conditions, the plate's surface was set as a viscous wall; a constant flow velocity combined with zero Neumann pressure condition was imposed at the inflow (semi-circular) and lateral (top and bottom) boundaries; at the outflow, a zero Dirichlet pressure condition was chosen along with a zero Neumann condition for the velocity, which is the default high-order outflow boundary condition available in $Nektar$++.

All simulations required GJP stabilization, as cases eventually showed numerical divergence at the adopted Reynolds number. With GJP, however, all cases remained stable and the numerical dissipation introduced did not show noticeable signs of solution quality degradation. In that sense, the GJP technique advocated in Section 2 showed excellent suitability for the vortex-dominated flow under study.

In Table 3, the results of Yang *et al.* (2012) are listed along with those obtained in the present study. As one can see, C_L and C_D values show discrepancies of approximately 4% and 11%, respectively. These differences are to be expected

if one takes into account that the simulations of Yang *et al.* (2012) relied on a finite difference scheme with the so-called immersed boundaries technique. The latter approximates boundaries (surfaces) with low-order accuracy and is typically expected to degrade solution quality in the vicinity of surfaces. Also, friction drag is often predicted with low accuracy. In fact, it is somewhat surprising to find that discrepancies are not even larger. As the simulations in the present work have been obtained with a more accurate and sophisticated method, it is natural to expect some differences when comparing results with those of Yang *et al.* (2012). For completeness, the temporal variations of C_L and C_D are shown in Fig. 5 over two complete shedding cycles.

Table 3: Comparison of lift and drag coefficients (mean and RMS fluctuation)

Simulation	$\overline{C_L}$	$\overline{C_D}$	C'_L	C'_D
Sharp edge	2.1109	1.3081	0.4032	0.1447
Rounded edge	2.0440	1.2763	0.4093	0.1442
Yang *et al.* (2012)	2.1156	1.1643	–	–

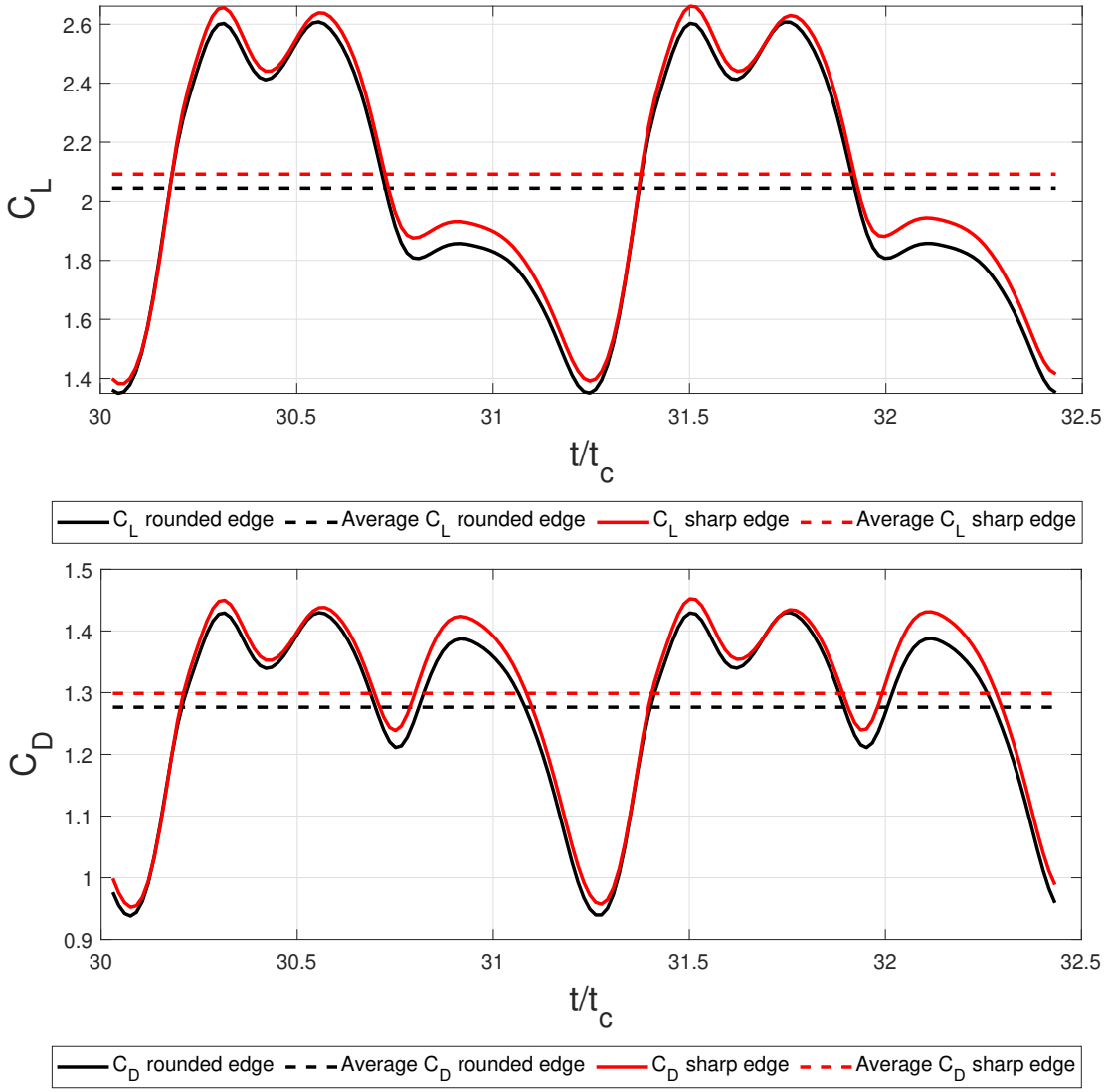

Figure 5: Temporal behavior of lift (upper) and drag (lower) coefficients over two complete shedding cycles.

Another comparison that can be made is that of pressure distribution, which is shown in Fig. 6. Error bars are used to indicate RMS fluctuations of measured C_P around mean values. The results obtained for both the sharp and the round-edged plates compare favourably with those of Yang *et al.* (2012) for a sharp-edged plate. It is worth noticing that RMS fluctuation values are stronger for the plate with round edges, as could be expected since the separating shear layers are likely to wander more freely during the vortex shedding cycle when not constricted by sharp edges. It is interesting to see that the spectral/hp element method seems actually capable of capturing such fine differences between the sharp and round geometries.

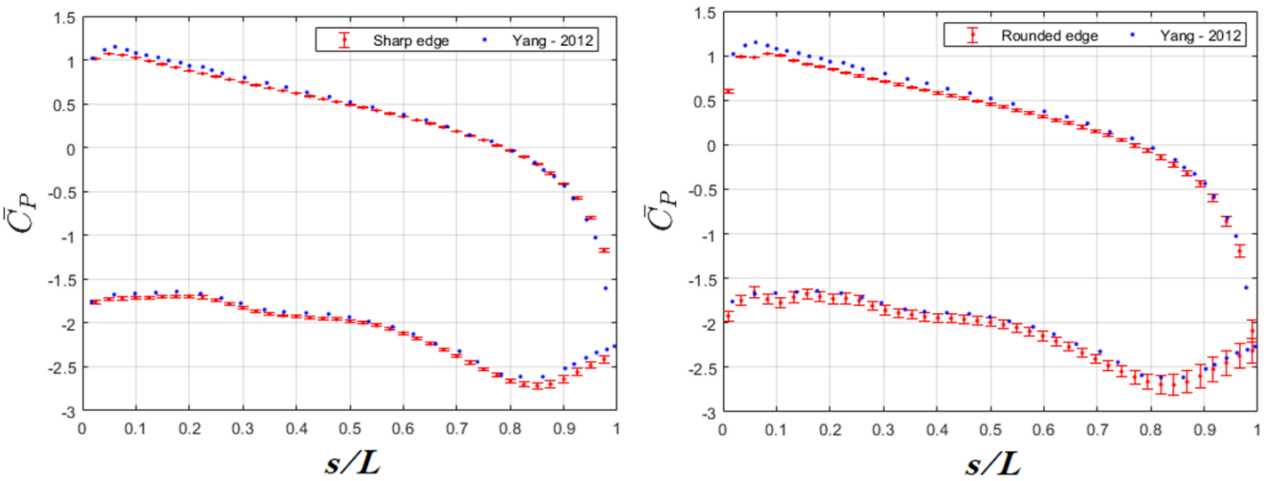

Figure 6: Pressure distribution for plates with sharp (left) and round edges (right), both compared with the results of Yang *et al.* (2012) for a sharp-edged plate (dark bullets). The error bars denote RMS fluctuation around the average C_P values.

This small differences between the two plates can also be observed in Fig. 7, which shows the instantaneous vorticity field in each case. The blue color in the plots denote clockwise rotation, whereas the red color denotes counter-clockwise rotation. As noted in Yang *et al.* (2012), there are two vortex being formed next to the leading edge. One of them goes downstream in pair with the vortex formed in the trailing edge. As this vortex pair travels downstream, it also rises in the vertical direction, following an oblique trajectory. The other vortex goes downstream alone and remains approximately at a fixed vertical coordinate ($y/L \approx -1$). Unlike the vortex pair, it remains vertically close to the point from which it was emitted. The results obtained here are in line with previous studies on 2D flat plate simulations, see also Li *et al.* (2017).

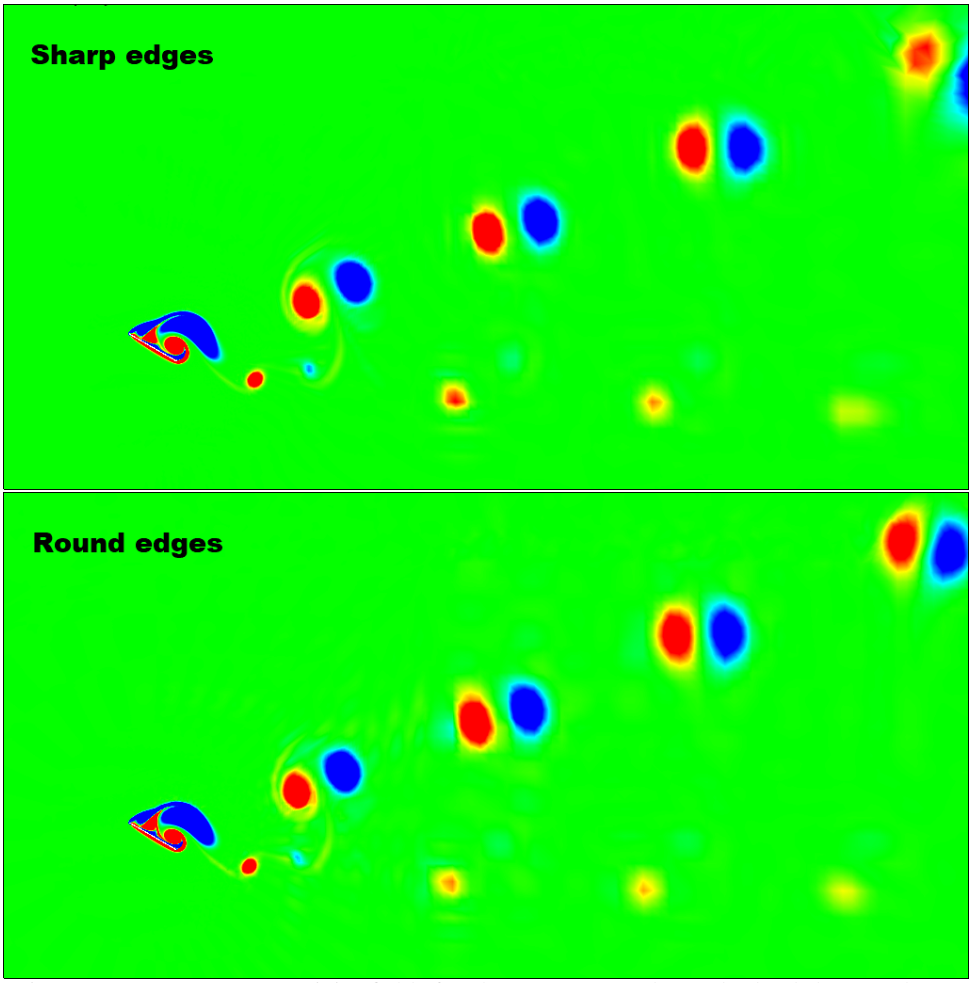

Figure 7: Instantaneous vorticity fields for sharp (upper) and round-edged (lower) plates.

5. CONCLUSIONS

In this work, a numerical study of the flow past an inclined flat plate was conducted. The simulations were run with a spectral/hp continuous Galerkin (CG) method with a novel stabilization technique. Specifically, this technique was an adapted version of the GJP (gradient-jump penalty) operator (Burman, 2007; Burman and Fernández, 2009; Burman, 2015) that is better suited for high-fidelity simulations of transitional and turbulent flows.

Adaptation of the GJP operator followed the estimates obtained with a linear dispersion/diffusion analysis (Mengaldo *et al.*, 2018a; Moura *et al.*, 2020a), which indicated substantial potential of the adapted operator for under-resolved simulations (Moura *et al.*, 2020b). The adapted GJP stabilization technique was tested with success and shown capable of stabilizing a vortex-dominated Navier-Stokes solution (inclined flat plate flow) at moderate Reynolds number without degrading CG's high-order accuracy.

The results found for an inclined plate at 30^o were consistent with the existing literature on the subject for both rounded and sharp edges. Some small differences in $\overline{C_L}$, $\overline{C_D}$ and $\overline{C_P}$ were found when comparing our results with those of Yang *et al.* (2012), but these can be safely attributed to higher accuracy of the numerical method employed in the present work. Our results confirmed that, for the test case considered (inclination of 30^o and $Re = 1000$), the vortices emitted from the leading edge propagate obliquely and form a wake that is ever expanding in the vertical direction. This observation is in line with previous works, such as that of Li *et al.* (2017).

6. ACKNOWLEDGEMENTS

The authors would like to thank Prof. Spencer J. Sherwin and Dr. Andrea Cassinelli from Imperial College London, which made the GJP stabilization strategy available in the $Nektar$++ framework, as well as Prof. Erik Burman from University College London for the helpful discussions about GJP stabilization theory. The authors gratefully acknowledge funding from São Paulo Research Foundation (FAPESP) under grant #2020/10910-8. In addition, Yukari W. G. Martins acknowledges funding from CNPq (Conselho Nacional de Desenvolvimento Científico e Tecnológico – Brasil).

7. REFERENCES

Amor, C., Pérez Pérez, J., Schlatter, P., Vinuesa, R. and Le Clainche, S., 2020. "Modeling the turbulent wake behind a wall-mounted square cylinder". *Logic Journal of IGPL*, pp. 1–11. doi:10.1093/OUP.

Breuer, M. and Jovicic, N., 2001. "Separated flow around a flat plate at high incidence: an les investigation". In *Second Symposium on Turbulence and Shear Flow Phenomena*. Begel House Inc.

Burman, E., 2007. "Interior penalty variational multiscale method for the incompressible navier–stokes equation: Monitoring artificial dissipation". *Computer methods in applied mechanics and engineering*, Vol. 196, No. 41-44, pp. 4045–4058.

Burman, E., 2015. "Robust error estimates for stabilized finite element approximations of the two dimensional navier–stokes' equations at high reynolds number". *Computer Methods in Applied Mechanics and Engineering*, Vol. 288, pp. 2–23.

Burman, E. and Fernández, M.A., 2009. "Finite element methods with symmetric stabilization for the transient convection–diffusion–reaction equation". *Computer Methods in Applied Mechanics and Engineering*, Vol. 198, No. 33-36, pp. 2508–2519.

Cantwell, C.D., Moxey, D., Comerford, A., Bolis, A., Rocco, G., Mengaldo, G., De Grazia, D., Yakovlev, S., Lombard, J.E., Ekelschot, D. *et al.*, 2015. "Nektar++: An open-source spectral/hp element framework". *Computer physics communications*, Vol. 192, pp. 205–219.

Fernandez, P., Moura, R.C., Mengaldo, G. and Peraire, J., 2019. "Non-modal analysis of spectral element methods: Towards accurate and robust large-eddy simulations". *Computer Methods in Applied Mechanics and Engineering*, Vol. 346, pp. 43–62.

Geuzaine, C. and Remacle, J.F., 2009. "Gmsh: a three-dimensional finite element mesh generator with built-in pre- and post-processing facilities". *International Journal for Numerical Methods in Engineering*, Vol. 79, pp. 1309–1331.

Karniadakis, G. and Sherwin, S., 2013. *Spectral/hp Element Methods for Computational Fluid Dynamics: Second Edition*, OUP Oxford. Numerical Mathematics and Scientific Computation. ISBN 9780199671366.

Kirby, R.M. and Sherwin, S.J., 2006. "Stabilisation of spectral/hp element methods through spectral vanishing viscosity: Application to fluid mechanics modelling". *Computer methods in applied mechanics and engineering*, Vol. 195, No. 23-24, pp. 3128–3144.

Lam, K.M. and Wei, C., 2010. "Numerical simulation of vortex shedding from an inclined flat plate". *Engineering Applications of computational fluid mechanics*, Vol. 4, No. 4, pp. 569–579.

Li, Z., Lan, C., Jia, L. and Ma, Y., 2017. "Ground effects on separated laminar flows past an inclined flat plate". *Theoretical and Computational Fluid Dynamics*, Vol. 31, No. 2, pp. 127–136.

Lombard, J.E.W., Moxey, D., Sherwin, S.J., Hoessler, J.F., Dhandapani, S. and Taylor, M.J., 2016. "Implicit large-eddy

simulation of a wingtip vortex". *AIAA Journal*, Vol. 54, No. 2, pp. 506–518.

Mengaldo, G., Moura, R.C., Giralda, B., Peiró, J. and Sherwin, S.J., 2018a. "Spatial eigensolution analysis of discontinuous galerkin schemes with practical insights for under-resolved computations and implicit les". *Computers & Fluids*, Vol. 169, pp. 349–364.

Mengaldo, G., De Grazia, D., Moura, R.C. and Sherwin, S.J., 2018b. "Spatial eigensolution analysis of energy-stable flux reconstruction schemes and influence of the numerical flux on accuracy and robustness". *Journal of Computational Physics*, Vol. 358, pp. 1–20.

Moura, R.C., Aman, M., Peiró, J. and Sherwin, S.J., 2020a. "Spatial eigenanalysis of spectral/hp continuous galerkin schemes and their stabilisation via DG-mimicking spectral vanishing viscosity for high reynolds number flows". *Journal of Computational Physics*, Vol. 406, p. 109112.

Moura, R.C., Mengaldo, G., Peiró, J. and Sherwin, S.J., 2017. "On the eddy-resolving capability of high-order discontinuous galerkin approaches to implicit les/under-resolved dns of euler turbulence". *Journal of Computational Physics*, Vol. 330, pp. 615–623.

Moura, R.C., Sherwin, S.J. and Peiró, J., 2015. "Linear dispersion–diffusion analysis and its application to under-resolved turbulence simulations using discontinuous galerkin spectral/hp methods". *Journal of Computational Physics*, Vol. 298, pp. 695–710.

Moura, R.C., Sherwin, S.J. and Peiró, J., 2016. "Eigensolution analysis of spectral/hp continuous galerkin approximations to advection–diffusion problems: Insights into spectral vanishing viscosity". *Journal of Computational Physics*, Vol. 307, pp. 401–422.

Moura, R.C., Silva, A.F.C. and Sherwin, S., 2020b. "Eigenanalysis of gradient-jump penalty (gjp) stabilisation for cg". *LASCA research report*. doi:10.13140/RG.2.2.32887.85924.

Moxey, D., Cantwell, C.D., Bao, Y., Cassinelli, A., Castiglioni, G., Chun, S., Juda, E., Kazemi, E., Lackhove, K., Marcon, J. *et al.*, 2020. "Nektar++: Enhancing the capability and application of high-fidelity spectral/hp element methods". *Computer Physics Communications*, Vol. 249, p. 107110.

Wang, Z.J., 2007. "High-order methods for the euler and navier–stokes equations on unstructured grids". *Progress in Aerospace Sciences*, Vol. 43, No. 1-3, pp. 1–41.

Xu, H., Cantwell, C.D., Monteserin, C., Eskilsson, C., Engsig-Karup, A.P. and Sherwin, S.J., 2018. "Spectral/hp element methods: Recent developments, applications, and perspectives". *Journal of Hydrodynamics*, Vol. 30, No. 1, pp. 1–22.

Yang, D., Pettersen, B., Andersson, H.I. and Narasimhamurthy, V.D., 2012. "Vortex shedding in flow past an inclined flat plate at high incidence". *Physics of Fluids*, Vol. 24, No. 8.

8. RESPONSIBILITY NOTICE

The authors are solely responsible for the printed material included in this paper.